Article

Not peer-reviewed version

A Flexible and Transparent PtNP/Swcnt/Pet Electrochemical Sensor for Nonenzymatic Detection of Hydrogen Peroxide Released From Living Cells With Real-time Monitoring Capability

Da Eun Oh , Chang-Seuk Lee , Tae Wan Kim , Seob Jeon , Tae Hyun Kim *

Posted Date: 7 June 2023

doi: 10.20944/preprints202306.0486.v1

Keywords: Electrochemical sensing; flexible sensor; hydrogen peroxide (H2O2); platinum nanoparticles; single-walled carbon nanotube (SWCNT) network

Article

A Flexible and Transparent PtNP/SWCNT/PET Electrochemical Sensor for Nonenzymatic Detection of Hydrogen Peroxide Released from Living Cells with Real-Time Monitoring Capability

Da Eun Oh [1,†], Chang-Seuk Lee [2,†], Tae Wan Kim [3], Seob Jeon [4] and Tae Hyun Kim [1,*]

[1] Department of Chemistry, Soonchunhyang University, Asan 31538, Republic of Korea
[2] Department of Chemistry, Seoul Woman's University, Seoul, 01797, Republic of Korea
[3] Department of Medical Life Science, Soonchunhyang University, Asan 31538, Republic of Korea
[4] Department of Obstetrics and Gynecology, College of Medicine, Soonchunhyang University Cheonan Hospital, Cheonan 31151, Republic of Korea
* Correspondence: thkim@sch.ac.kr
† These authors contributed equally to this work.

Abstract: We developed a transparent and flexible electrochemical sensor using a platform based on a network of single-walled carbon nanotubes (SWCNTs) for the non-enzymatic detection of hydrogen peroxide (H_2O_2) released from living cells. We decorated the SWCNT network on a poly(ethylene terephthalate) (PET) substrate with platinum nanoparticles (PtNPs) using a potentiodynamic method. The PtNP/SWCNT/PET sensor synergized the advantages of a flexible PET substrate, a conducting SWCNT network, and a catalytic PtNP, and demonstrated good biocompatibility and flexibility, enabling cell adhesion. The PtNP/SWCNT/PET-based sensor demonstrated enhanced electrocatalytic activity towards H_2O_2 as well as excellent selectivity, stability, and reproducibility. The sensor exhibited a wide dynamic range of 500 nM to 1 M, with a low detection limit of 228 nM. In addition, Furthermore, the PtNP/SWCNT/PET sensor remained operationally stable even after bending at various angles (15°, 30°, 60°, and 90°) with no noticeable loss of current signal. These outstanding characteristics enabled the PtNP/SWCNT/PET sensor to be practically applied for the direct culture of HeLa cells and the real-time monitoring of H_2O_2 release by the HeLa cells under drug stimulation.

Keywords: Electrochemical sensing; flexible sensor; hydrogen peroxide (H_2O_2); platinum nanoparticles; single-walled carbon nanotube (SWCNT) network

1. Introduction

With the rapid development of wearable electronic devices, flexible electrodes are increasingly in demand since they can conform to different forms and surfaces, such as human skin and other biological tissues [1,2]. Flexible electrodes have potential applications in point-of-care tests and wearable biosensing systems which allow in situ quantification of various biochemical elements present in the human body, thus promising personalized health monitoring [3–5]. Flexible electrodes provide several benefits over conventional electrodes as supports of biosensing platforms such as conformability, light weight, portability, low cost, wearability, and facile integration into the transformable system [6–8]. To fabricate a high-performance flexible biosensor, the electrode materials should possess chemical or biological functionality such as catalytic activity, biocompatibility, and chemical stability, along with physical characteristics, such as flexibility and transparency [9–11]. Thus, various nanomaterials, including carbon nanomaterials, metal nanowires, conducting polymers, and their composites, have been employed as electrode materials coated on flexible supports (plastic, paper, and textiles) [12–20]. We previously reported transparent flexible electrodes based on a single-walled carbon nanotube (SWCNT) network using a poly(ethylene terephthalate) (PET) film substrate for the construction of flexible electrochemical biosensors [21,22].

 doi:10.20944/preprints202306.0486.v1

We used electrochemical approaches, in particular, to prepare the electrochemically-doped SWCNT film electrode or dendrimer-grafted SWCNT film electrode, which demonstrated catalytic activity in chemical and biological reactions without the loss of flexibility and transparency.

In order to broaden the scope of our research developing facile SWCNT-based flexible sensing platforms, herein, we demonstrate in situ monitoring of hydrogen peroxide (H_2O_2) released from living cells using a functionalized SWCNT/PET film electrode. As a momentous part of reactive oxygen species (ROS), H_2O_2 is generated from cellular metabolism and serves as a signaling molecule that modulates a variety of biological processes in the human body, including cell migration, proliferation, and differentiation under physiological conditions [23,24]. In cellular environments, overgeneration of H_2O_2, however, can disrupt the cellular redox homeostasis, leading to destructive oxidative stress, since its long lifetime allows it to penetrate other cellular compartments and to be accumulated [25]. Consequently, an abnormal level of H_2O_2 causes various pathological events, such as cancer, heart attack, aging, Parkinson's disease, and Alzheimer's disease [26–29]. Therefore, the selective and quantitative detection of cellular H_2O_2 and monitoring of its dynamic release process from living cells can not only help elucidate its roles in cellular physiology but also provide a reliable diagnosis of pathological conditions.

Currently, to detect H_2O_2 in the cellular environment, a variety of sensors have been developed based on different analytical techniques [30–35]. Among them, the electrochemical method offers the advantages of low cost, fast response, high sensitivity, simple instrumentation, and label-free detection [36–43]. Many electrochemical sensors have been developed for direct and real-time detection of cellular H_2O_2 using different electrodes based on emerging materials, such as graphene [40,43,44], Au–TiO_2 [38], MoS_2 nanoparticles [41], Mn_2CuO_4 microspheres [36], $ZnMn_2O_4$@rGO/GCE [39], GO-AuNP/ITO [37], etc. However, most sensors are often made with firm and rigid electrodes which are unsatisfactory to comply with elastic and curved cells. Since mechanical stress caused by the contact between cells and substrate could influence the H_2O_2 expression of the cells [45–47], flexible electrodes should be suitable substrates for enhanced biocompatibility, improved cell adhesion, increased stability during cell culture, and thereby monitoring H_2O_2 released from the cells.

SWCNT offers several advantages for biosensors, including high electronic conductivity, little surface fouling, chemical stability, and high sensitivity due to the one-dimensional quantum confinement properties [48,49]. Moreover, SWCNTs integrated into PET (SWCNT/PET) offer flexibility, transparency, and transducing capability, making them attractive for wearable biosensors [50,51]. However, SWCNT/PET electrode lacks catalytic activity toward H_2O_2.

To address this issue, we functionalized the SWCNT/PET film electrode with platinum nanoparticles (PtNPs) to develop a non-enzymatic, flexible electrochemical sensor for in situ monitoring of H_2O_2 (Scheme 1). The PtNPs improve conductivity and biocompatibility of the film, while their inherent electrocatalytic activity toward H_2O_2 enables the sensitive and selective detection of H_2O_2 [52–54]. The SWCNT network also acts as a stable conductive substrate that maintains stability under mechanical stress. This substrate also offers several advantages over traditional rigid substrates, including improved flexibility, biocompatibility, and transparency. These features enable real-time monitoring of H_2O_2 release from living cells, which is critical for understanding the dynamics of cellular processes.

Overall, flexible substrates represent a significant advancement in the field of electrochemical sensing, particularly for applications involving living cells. Our work demonstrates the potential of flexible substrates for real-time monitoring of H_2O_2 release from living cells and highlights the importance of using appropriate substrates for successful electrochemical sensing in biological systems.

Preprints (www.preprints.org) | NOT PEER-REVIEWED | Posted: 7 June 2023 doi:10.20944/preprints202306.0486.v1

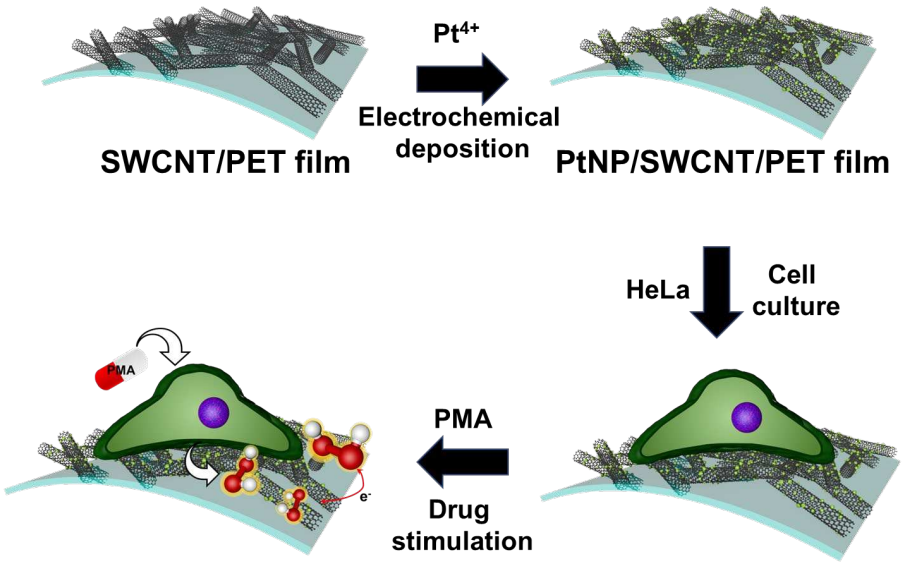

Scheme 1. Fabrication of a flexible electrochemical sensor based on SWCNT/PET film functionalized with PtNP and its sensing principle for real-time monitoring of H_2O_2 release from living cells.

2. Materials and Methods

2.1. Materials

Chloroplatinic acid hexahydrate ($H_2PtCl_6 \bullet 6H_2O$), potassium ferricyanide ($K_3Fe(CN)_6$), sulfuric acid (H_2SO_4), Phorbol 12-myristate 13-acetate (PMA), glucose, cysteine, 4-acetamidophenol, glutamic acid, dopamine (DA), L-(+)-ascorbic acid (AA), uric acid (UA), acetone, methanol, and phosphate buffer saline (PBS) were purchased from Sigma-Aldrich. Hydrogen peroxide (H_2O_2) was obtained from Samchun pure chemical co, LTD. H_2O_2 is prepared in 10 mM phosphate buffer saline (PBS) solutions at pH 7.4. All chemicals used were of analytical grades and aqueous solutions were prepared with deionized (DI) water. DI water was prepared using water purification systems (specific resistivity >18 MΩ cm, Milli-Q, Millipore Korea, Co., Ltd., aqua Max Ultra 370, Younglin Instrument Co., Anyang, Gyounggi-do, Korea). Hoechst 33342 Trihydrochloride trihydrate (Hoechst 33342) was obtained from Thermo Fisher scientific. AZ 5214-E photoresist (PR) and AZ 300 MIF Developer were purchased from AZ Electronic Materials (Luxembourg, UK).

2.2. Instrumentation

All electrochemical measurements were performed using a CHI 760E electrochemical workstation (CH Instruments, Inc., USA). The working electrode used was a flexible SWCNT/PET film, which was prepared by coating SWCNT onto a flexible poly(ethylene terephthalate) (PET) substrate using a vacuum filtration method (Topnanosys Co., Cheonan, Chungcheongnam-do, South Korea). A platinum wire and an Ag/AgCl electrode (saturated KCl) were employed as the counter electrode and reference electrode, respectively. Contact angle measurements were performed on a PHOENIX-MINI (SEO Co, Ltd., Suwon, Gyeonggi-do, Korea). FE-SEM images and EDX spectrum were taken on a SIGMA500 (Carl ZEISS, Jena, Germany 1846). The biocompatibility images were obtained by confocal microscopy FV-10i (Olympus Co., Ltd. Shinjuku-ku, Tokyo, Japan). The optical transmittances of SWCNT network films were recorded by an ultraviolet-visible-near infrared (UV–vis-NIR) spectrophotometer V-670 (Jasco International Co., Ltd., Hachioji City, Tokyo, Japan).

 doi:10.20944/preprints202306.0486.v1

2.3. Fabrication of PtNP/SWCNT/PET network film electrode

To synthesize and deposit PtNPs on the SWCNT film, the film was immersed in DI water containing 1.0 mg/mL Pt^{4+} ion. Electrodeposition of Pt was performed by cyclic voltammetry (CV) technique at a scan rate of 50 mV/s for 20 cycles, using a potential range of -0.2 V to 0.8 V. After being rinsed with DI water and dried with N_2 gas, the PtNP/SWCNT network film electrode was obtained. The geometrical surface area of the working electrode was 0.0706 cm^2. For comparative study to monitor H_2O_2 release from cells in real time, interdigitated array electrodes (IDE) with different pairs of PtNP/SWCNT and/or bare SWCNT electrodes were fabricated. The IDE was composed of 16 electrode fingers with a width of 100 μm, gap of 100 μm, and length of 1.95 mm. The IDE was patterned on the SWCNT/PET film using the standard photolithography method. The SWCNT film was first deposited with AZ 5214-E PR through spin coating process with 3000 rpm for 30 sec, resulting in a film thickness of 1.62 μm. The film was then soft baked at 80 °C for 1 min to remove moisture on the surface of substrate and remove the standing wave on the positive PR layer. Next, UV light exposure was conducted for 30 sec to pattern transfer the IDE mask on the SWCNT/PET film surface. For the development process, AZ 300 MIF developer was used twice at room temperature for 10 min. Finally, etching process using O_2 plasma for 20 min was carried out to remove an unexposed area.

2.4. Cell culture and imaging

The human cervical cancer cell line HeLa was obtained from the Korean cell line bank (KCLB, Seoul, Korea). Cells were grown in Roswell Park Memorial Institute (RPMI) 1640 medium (Cellgro, Manassas, VA, USA) supplemented with 10% fetal bovine serum (FBS; Equitech-bio, Kerrville, TX, USA), 1% penicillin–streptomycin (APS) at 37 °C in a humidified atmosphere containing 5% CO_2. To test the cell viability, the PtNP/SWCNT network film (1.5 cm × 3 cm) was prepared and sterilized by irradiating it with UV for 2 h before seeding the cells. Then, HeLa cells at a density of ~5×10^4 cell cm^{-2} were seeded on the PtNP/SWCNT network film electrode. After 24 h, 48 h, and 72 h of incubation, the cells were stained with Hoechst 33342 for fluorescence imaging to compare the biocompatibility.

3. Results

3.1. Preparation and characterization of PtNP/SWCNT network film

A trasparent and flexible SWCNT network film was functionalized with PtNPs via electrochemical deposition with a potential range of -0.2 V to 0.8 V in a 0.1 mg/mL Pt^{4+} aqueous solution for 20 cycles using CV method. As shown in Figure S1 (Supplementary Material), the oxidation and reduction currents gradually increased with each scan cycle. After the redox process with multiple CV scans, PtNPs were successfully formed on the SWCNT network film, while the SWCNTs remained well-distributed and networked each other on a PET film without any discernible morphological change in the FE-SEM images (Figure 1A). To confirm the presence of PtNPs on the SWCNT surface, the elemental compositions were analyzed using EDS (Figure 1B). The EDS spectrum showed characteristic signals of C, O, and Pt, which identified the formation of PtNPs via electrochemical deposition on the SWCNT network film. The corresponding particle size distribution histogram is shown in Figure 1C, and the measured size of PtNPs was 360 nm ± 70 nm for the average diameter with standard deviation. Figure 1D displays the flexible system based on PtNP/SWCNT network films showing high transparency with a transmittance value of around 80% in the Vis-NIR range (Figure S2). As shown in Figure S2, the transmittance did not change significantly after the electrodeposition process of PtNPs on SWCNT network films.

The electron transfer kinetics of the PtNP/SWCNT network film were studied by voltammetric and impedimetric measurements utilizing $[Fe(CN)_6]^{3-}$ as a redox probe. Figure 2A shows the voltammetric responses of bare SWCNT and PtNP/SWCNT films in 0.1 M KCl containing 10 mM $[Fe(CN)_6]^{3-}$. The bare SWCNT film exhibited a pair of redox peaks with peak-to-peak separation (ΔE_p) of 0.62 V, which suggests a quasi-reversible process attributable to the slow diffusion through the

Preprints (www.preprints.org) | NOT PEER-REVIEWED | Posted: 7 June 2023 doi:10.20944/preprints202306.0486.v1

narrow pores and the sluggish electron transfer at the SWCNT surface caused by graphite basal plane-like structure [55]. On the contrary, PtNP/SWCNT network film showed better electrochemical performance with a smaller ΔE_p of 0.26 V and enhanced redox redox peak currents (i_p). This is owing to the electrocatalytic effect of PtNPs and the large effective surface area of the PtNP/SWCNT film. The effective surface area of the PtNP/SWCNT network film was determined from CV curves obtained from 0.1 M KCl containing 10 mM $[Fe(CN)_6]^{3-}$ at varying scan rates. The corresponding plot (Figure 2B) showed a linear relation between i_p and the root squared of the scan rate, which is consistent with the Randles-Sevick model for diffusion-controlled transport of species. The determined surface area of the PtNP/SWCNT film was 0.097 cm^2, which is larger than that of bare SWCNT film (0.055 cm^2). EIS measurements also confirm the formation of PtNP on the SWCNT surface and the better electrocatalytic behavior of the PtNP/SWCNT network film, compared with the bare SWCNT film (Figure 2C). The Nyquist plots demonstrated a significant drop in the diameter of the semicircle after the electrodeposition of PtNP on SWCNT surface, indicating a decrease in the charge transfer resistance (R_{ct}) and an enhanced electron transfer of the redox probe at PtNP/SWCNT surface. The values of R_{ct}, calculated from semicircle in the high frequency region of Nyquist plot, were 5.47 kΩ and 7.75 kΩ for PtNP/SWCNT and bare SWCNT films, respectively. The lower impedance interface of the PtNP/SWCNT films was mainly attributed to the higher conductivity of the electrodeposited platinum. Since cell adhesion and interaction onto the electrode substrate depends on the hydrophilicity of the surface of electrode, the wetting contact angle of the PtNP/SWCNT films was investigated. The wetting characteristics of bare SWCNT and PtNP/SWCNT network films are shown in Figure 2D, where the average equilibrium static contact angles were found to be 97° and 82°, respectively. The electrodeposition of PtNPs on the SWCNT film resulted in a more hydrophilic surface, which may be attributed to the hydrophilic property of PtNPs [56], as well as the enhanced roughness of the film surface.

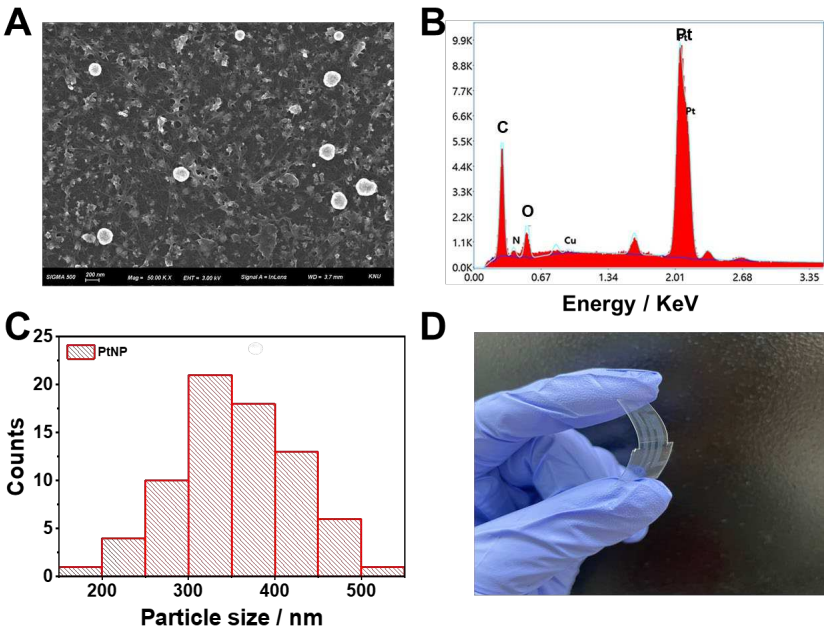

Figure 1. (A) FE-SEM image and (B) EDX spectrum of PtNP/SWCNT network film. (C) Histogram of particle size distribution of PtNP. (D) Photograph of bent PtNP/SWCNT network film.

Preprints (www.preprints.org) | NOT PEER-REVIEWED | Posted: 7 June 2023 doi:10.20944/preprints202306.0486.v1

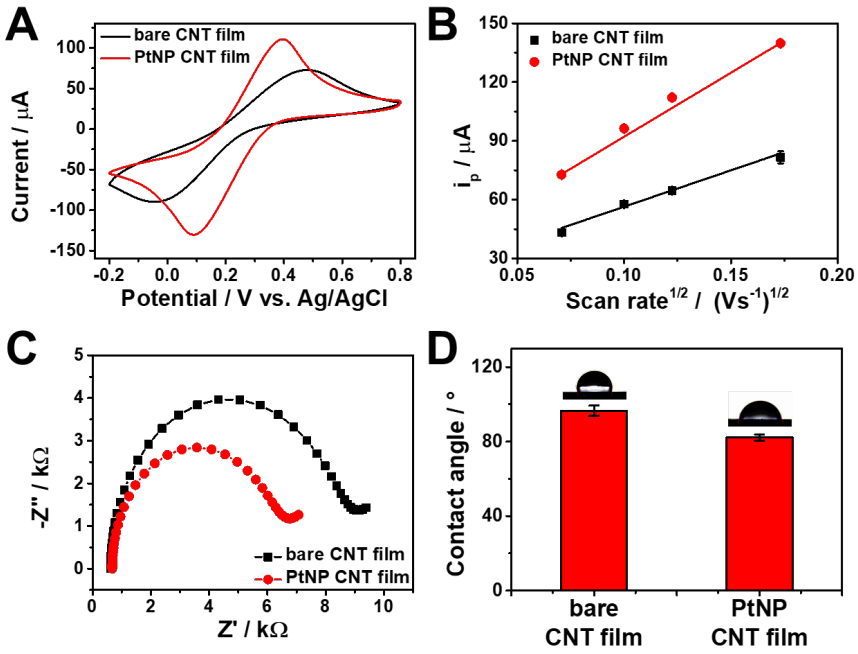

Figure 2. (A) CV curves of bare SWCNT and PtNP/SWCNT network film in 0.1 M KCl containing 10 mM $[Fe(CN)_6]^{3-}$ at a scan rate of 15 mV/s. (B) The corresponding plots for cathodic peak currents vs. the square root of scan rate. (C) Nyquist plots of bare SWCNT film, and PtNP/SWCNT film in 0.1 M KCl containing 10 mM $[Fe(CN)_6]^{3-}$. (D) Contact angle measurements. Images of a water droplet on the surfaces of bare SWCNT film and PtNP/SWCNT film.

3.2. Electrochemical sensing performance toward H_2O_2

In order to investigate the impact of Pt on the sensor's performance, we compared the electrochemical catalytic behavior of the PtNP/SWCNT network film with that of the bare SWCNT film using CV. Figure 3A shows the voltammetric responses toward 1 mM of H_2O_2 in 10 mM PBS at pH 7.4. No noticeable signal was detected in the absence of H_2O_2 for both bare SWCNT and PtNP/SWCNT network films. However, the addition of 1 mM H_2O_2 resulted in significant redox currents, originating from the catalytic oxidation and reduction of H_2O_2 at the surface of the electrode. Notably, the current response of the PtNP/SWCNT network film was much higher than that of the bare SWCNT. This improvement in electrocatalytic activity is attributed to the higher electrocatalytic performance and good conductivity of the PtNPs deposited on the SWCNT films. These results demonstrate the potential of flexible and transparent PtNP/SWCNT network film for the detection of H_2O_2. It is worth noting that the electrodeposition of PtNPs on the SWCNT surface was further confirmed by the altered electrocatalytic activity of the SWCNT film for H_2O_2 redox processes.

To assess the analytical performance of the PtNP/SWCNT network film, we conducted chronoamperometric measurements in 10 mM PBS. The working potential applied was 0.6 V, where H_2O_2 oxidizes. The oxidation of H_2O_2 is more sensitive and reproducible compared to its reduction since oxygen does not contribute to the background current [57,58]. On the other hand, the reduction of H_2O_2 at a negative potential may have difficulty in obtaining a reproducible amperometric signal since the H_2O_2 signal would be obscured by the oxygen reduction [57]. Figure 3B displays the typical amperometric responses of the PtNP/SWCNT network film alongside the bare SWCNT film upon adding H_2O_2 at a selected working potential of 0.6 V. The PtNP/SWCNT network film electrode exhibits highly sensitive amperometric responses, compared to the bare SWCNT film. The electrode showed a quick current response that could achieve a dynamic equilibrium of current signal under 5 seconds after adding H_2O_2, reflecting a favorable electron transfer between PtNP/SWCNT network film and H_2O_2. H_2O_2 began to trigger a response from the PtNP/SWCNT network film at a concentration of 500 nM, and subsequent additions of H_2O_2 resulted in proportional increases in current. Figure 3C shows the calibration curve for H_2O_2 measurements with PtNP/SWCNT network

Preprints (www.preprints.org) | NOT PEER-REVIEWED | Posted: 7 June 2023 doi:10.20944/preprints202306.0486.v1

film sensor, demonstrating a wide dynamic range (500 nM-1 M) in which there were detectable signals and a highly sensitive linear range with a steep slope of approximately 44 per decade. For the linear range, the regression equation is represented as i (μA) = 156 + 44.2 log [H_2O_2] (M) (correlation coefficient, R^2 = 0.982). The limit of detection (LOD) of the sensor for H_2O_2 were estimated to be 228 nM at a signal-to-noise (S/N) ratio of 3, demonstrating superior electrochemical sensing ability compared to the bare SWCNT film (LOD = 14.0 μM). To assess the selectivity of the sensor, we tested its amperometric responses upon the addition of H_2O_2 and several other biochemical species, including cysteine, 4-acetamidophenol, glutamic acid, dopamine, ascorbic acid, and uric acid. As shown in Figure 3D, only the introduction of H_2O_2 resulted in a noticeable change in the amperometric response, while other biochemical species, even at concentrations ten times higher, produced no discernible effect, indicating excellent selectivity of the sensor. We also evaluated the reproducibility of the fabricated sensors by recording CV curves of 1 mM H_2O_2 at five different PtNP/SWCNT network electrodes prepared under identical conditions. As depicted in Figure 3E, the anodic peak currents at 0.6 V showed an average relative standard deviation (RSD) of only 0.7%, demonstrating the sensors' reproducibility. Furthermore, we examined the effects of bending stress on the overall sensing performance of the PtNP/SWCNT network film, as flexibility is critical for practical biosensor devices. The sensor showed negligible changes when bent inward at angles of 15°, 30°, 60°, and 90°, with an average RSD of 1.3% in the amperometric response towards 100 μM H_2O_2. The sensor's stability under bending cycles was also evaluated using a home-made bending apparatus. The bending cycle stability of the PtNP/SWCNT network film electrode was evaluated up to 500 bending cycles at 60° in Figure S3, demonstrating excellent stability with approximately 95% signal retention after 300 cycles and 84% signal retention after 500 cycles of bending.

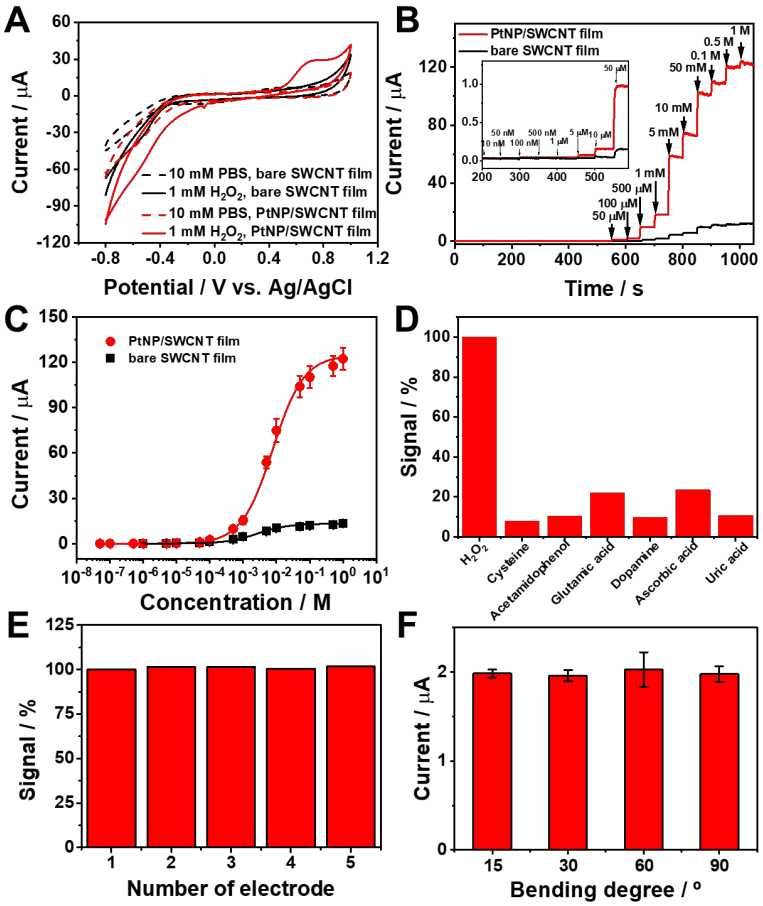

Figure 3. (A) CV curves of bare SWCNT (black line) and PtNP/SWCNT (red line) network films in 10 mM PBS (pH 7.4) in the absence (dashed line) and the presence (solid line) of 1 mM H_2O_2 at a scan rate of 50 mV/s. (B) Amperometric responses of bare SWCNT (black line) and PtNP/SWCNT (red line) network films to successive addition of H_2O_2 to PBS (10 mM, pH 7.4) at a fixed potential of 0.6 V under

stirring, and (C) the corresponding calibration curves. (D) Selectivity of PtNP/SWCNT network film sensor. Signals were compared from each amperometric current of 10 μM H_2O_2, 100 μM cysteine, 4-acetamidopenol, glutamic acid, dopamine, ascorbic acid, and uric acid to PBS (10 mM, pH 7.4) at a fixed potential of 0.6 V under stirring. (E) Sensor reproducibility for five different modified electrodes. Signals were compared from each i_p in the CV curves of 1 mM H_2O_2 at 0.6 V. (F) Effects of different bending angles (15, 30, 60, and 90°) on the current response to 100 μM H_2O_2 using the flexible PtNP/SWCNT film.

3.3. Real-time monitoring of H_2O_2 release from living cells

HeLa cells were cultured on the surface of the sterilized PtNP/SWCNT network film to show the viability of the PtNP/SWCNT network film as a flexible sensor for the in situ monitoring of cell exocytosis. The sensor's biocompatibility was first examined by fluorescence and microscope images. Figure 4 shows the images of HeLa cells seeded on the sensor for the cultivation of 24 h, 48 h, and 72 h. After 24 h, HeLa cells on the sensor formed pseudopodia and were firmly adhered to the surface. After 48 hours of culture, the cells grew and proliferated well on the surface, with most cells exhibiting their typical spindle structure. As the culture progressed until 72 h, HeLa cells with a spindle shape continued to proliferate effectively and nearly cover the whole surface. Fluorescence images clearly showed that most cells stained by Hoechst 33342 (cyan) were alive on the surface, demonstrating the sensor's outstanding biocompatibility for the adhesion and growth of the mammalian cells.

Along with the advantageous properties including flexibility, transparency, large surface area, good biocompatibility, and high conductivity, the PtNP/SWCNT film can be patterned into various shapes. Therefore, we prepared IDE sensors with three different electrode patterns using a standard photolithography method: pairs of PtNP/SWCNTs, pairs of bare SWCNTs, and pairs of half bare SWCNT and half PtNP/SWCNT. These sensors were used to monitor H_2O_2 release from HeLa cells cultured on the electrode surface by the amperometric method. Figure 5A displays the fabricated IDEs with different electrode pairs of PtNP/SWCNT and bare SWCNT. For in situ monitoring of H_2O_2 released from live cells, HeLa cells were cultured on the fabricated IDEs (Figure 5A(b-d)). The generation of H_2O_2 from HeLa cells was induced by adding PMA as a common stimulant which activates a series of signaling pathways including the oxidation of O_2, the generation of O_2^-, and finally the release of H_2O_2 to the extracellular environment [59,60]. Figure 5B shows a sharp increase of current on the IDE with pairs of PtNP/SWCNTs upon the addition of 100 μM PMA. To confirm that this current increase was caused by H_2O_2, 100 μM H_2O_2 was added, which led to a similar current increase, suggesting that the current response was due to the oxidation of H_2O_2 released from the HeLa cells cultured therein. In contrast, the IDE with pairs of bare SWCNTs exhibited a negligible current increase after the addition of the same amount of PMA and even H_2O_2 (Figure 5C), indicating the significance and electrocatalytic effect of PtNPs on the SWCNT film. In the case of the IDE with pairs of half PtNP/SWCNT and half bare SWCNT, upon the stimulation of PMA, the HeLa cells produced a distinct amperometric signal immediately only on the PtNP/SWCNT pattern (black line in Figure 5D). On the bare SWCNT pattern, the measured response was insignificant (red line in Figure 5D), reflecting the superior sensing capability of PtNP/SWCNT network film for real-time monitoring of H_2O_2 released from the cells.

To evaluate the flexibility of the PtNP/SWCNT film sensor in detecting biochemical signals from mechanically deformed cells, we tested its performance in real-time and in situ monitoring of H_2O_2 even when bent. Different mechanical bending strains were applied to the sensor with HeLa cells cultured on it. Figure 6 shows amperometric responses of cell-cultured PtNP/SWCNT film sensors under different bending states at angles of 15°, 30°, 45°, and 60° upon the addition of 100 μM PMA and H_2O_2 at 0.6 V in 10 mM PBS (pH 7.4). PMA stimulation still caused a significant current increase on all sensors under different bending states (Figure 6A-D), which is attributed to the H_2O_2 secreted from the cells. This indicates the cells at the deformed states could secrete H_2O_2. In addition, a staircase increase in current was observed upon the following successive addition of H_2O_2, suggesting that mechanical deformation has little effect on real-time and in situ monitoring of H_2O_2.

Preprints (www.preprints.org) | NOT PEER-REVIEWED | Posted: 7 June 2023 doi:10.20944/preprints202306.0486.v1

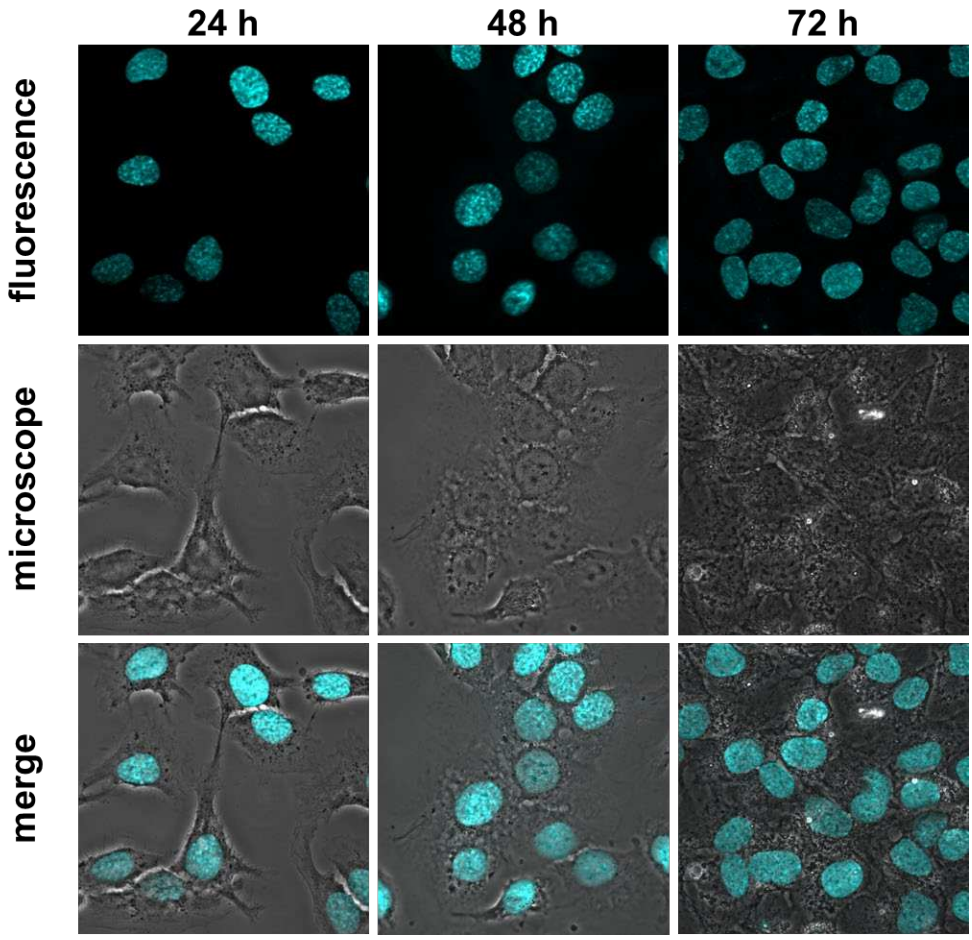

Figure 4. Fluorescence and microscopic for the biocompatibility test of HeLa cells cultured on PtNP/SWCNT network film for 24 h, 48 h, and 72 h. Cyan color represents Hoechst 33342 stained nuclei observed at 440-480 nm with 358 nm excitation.

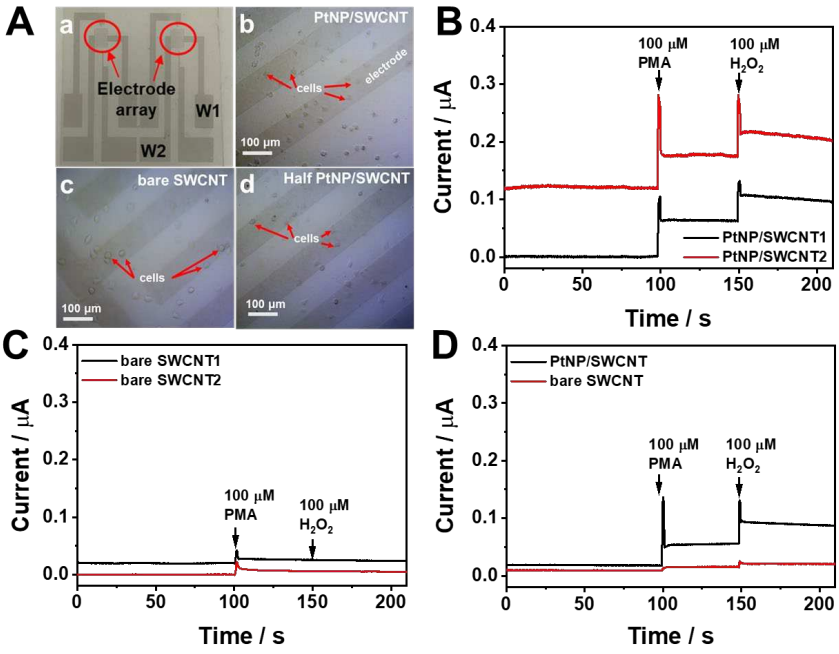

Figure 5. (A) (a) Photograph of IDEs, and magnifying images of IDE patterns with (b) pairs of PtNP/SWCNTs, (c) pairs of bare SWCNTs, and (d) pairs of half bare SWCNT and half PtNP/SWCNT,

Preprints (www.preprints.org) | NOT PEER-REVIEWED | Posted: 7 June 2023 doi:10.20944/preprints202306.0486.v1

cultured with HeLa cells. Monitoring of H_2O_2 release from HeLa cells using IDEs with (B) pattern (b), (C) pattern (c), and (D) pattern (d) upon the addition of 100 μM PMA at 0.6 V in 10 mM PBS (pH 7.4).

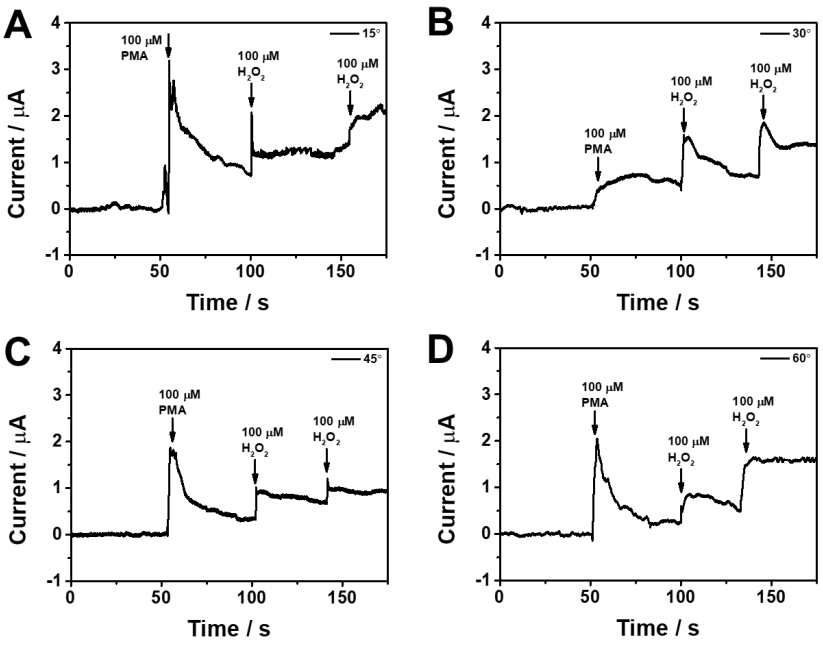

Figure 6. Monitoring of H_2O_2 release from HeLa cells using the PtNP/SWCNT network film sensor upon the addition of 100 μM PMA at 0.6 V in 10 mM PBS (pH 7.4) under different bending states at angles of (A) 15°, (B) 30°, (C) 45°, and (D) 60°.

4. Conclusions

Real time and in situ monitoring of H_2O_2 release from living cells was successfully achieved using a flexible and transparent PtNP/SWCNT network electrode. The electrode was fabricated by the electrodeposition of PtNPs on the SWCNT/PET film after multiple CV cycles. The resulting electrode demonstrated remarkable mechanical, physicochemical, and electrochemical properties due to the synergistic impact of different components in the PtNP/SWCNT network film, which led to enhanced non-enzymatic H_2O_2 detection. The electrode also showed good biocompatibility enabling conformal cell growth on its surface with excellent adhesion. These features allowed in situ tracking of H_2O_2 secreted from live cells under steady, or mechanically deformed states. This approach offers a promising strategy to develop flexible and transparent sensors for real time and in situ monitoring of electroactive species related to cell metabolism and for various biomedical applications. Moreover, it could serve as a potent tool for developing wearable biosensing devices in the future.

5. Patents

Supplementary Materials: The following supporting information can be downloaded at: www.mdpi.com/xxx/s1, Figure S1: CV curves of SWCNT/PET film electrode in 1 mg/mL chloroplatinic acid hexahydrate at a scan rate of 50 mV for 20 cycles.; Figure S2: Transmittance of bare SWCNT, flat PtNP/SWCNT film, and bent PtNP/SWCNT film.; Figure S3: Effects of bending cycles on the current response to 100 μM H_2O_2 using PtNP/SWCNT film bending at 60°.

Author Contributions: Conceptualization, Chang-Seuk Lee; Data curation, Da Eun Oh; Funding acquisition, Tae Hyun Kim; Investigation, Da Eun Oh and Chang-Seuk Lee; Resources, Tae Wan Kim and Seob Jeon; Supervision, Tae Hyun Kim; Writing – original draft, Tae Hyun Kim; Writing – review & editing, Tae Hyun Kim All authors have read and agreed to the published version of the manuscript.

Funding: This work was supported by Basic Science Research Program through the National Research Foundation of Korea (NRF), with the grant funded by Korea Government (MSIT) (No. NRF-2020R1A2C1014918) and (MOE) (NRF-2021R1A6A1A03039503). This work was conducted with the support of the Korea

Environment Industry & Technology Institute (KEITI) through its Ecological Imitation-based Environmental Pollution Management Technology Development Project and funded by the Korea Ministry of Environment (ME) (2019002800006). This work was also supported by the Soonchunhyang University Research Fund.

Institutional Review Board Statement: Not applicable.

Informed Consent Statement: Not applicable.

Data Availability Statement: The data that support the findings of this study are available from the corresponding author upon reasonable request.

Conflicts of Interest: The authors declare no conflict of interest.

References

1. Liu, Y.-L.; Huang, W.-H. Stretchable Electrochemical Sensors for Cell and Tissue Detection. *Angew. Chem.* **2021**, *133*, 2789–2799, doi:10.1002/ange.202007754.
2. Zhao, S.; Li, J.; Cao, D.; Zhang, G.; Li, J.; Li, K.; Yang, Y.; Wang, W.; Jin, Y.; Sun, R.; et al. Recent Advancements in Flexible and Stretchable Electrodes for Electromechanical Sensors: Strategies, Materials, and Features. *ACS Appl. Mater. Interfaces* **2017**, *9*, 12147–12164, doi:10.1021/acsami.6b13800.
3. Bandodkar, A.J.; Wang, J. Non-Invasive Wearable Electrochemical Sensors: A Review. *Trends Biotechnol.* **2014**, *32*, 363–371, doi:10.1016/j.tibtech.2014.04.005.
4. Kim, B.-Y.; Lee, H.-B.; Lee, N.-E. A Durable, Stretchable, and Disposable Electrochemical Biosensor on Three-Dimensional Micro-Patterned Stretchable Substrate. *Sens. Actuators B Chem.* **2019**, *283*, 312–320, doi:10.1016/j.snb.2018.12.045.
5. Flexible Sensors for Biomedical Technology - Lab on a Chip (RSC Publishing) DOI:10.1039/C5LC90136G Available online: https://pubs.rsc.org/en/content/articlehtml/2016/lc/c5lc90136g (accessed on 30 May 2023).
6. Chen, C.-H.; Lin, C.-T.; Hsu, W.-L.; Chang, Y.-C.; Yeh, S.-R.; Li, L.-J.; Yao, D.-J. A Flexible Hydrophilic-Modified Graphene Microprobe for Neural and Cardiac Recording. *Nanomedicine Nanotechnol. Biol. Med.* **2013**, *9*, 600–604, doi:10.1016/j.nano.2012.12.004.
7. Lou, C.; Li, R.; Li, Z.; Liang, T.; Wei, Z.; Run, M.; Yan, X.; Liu, X. Flexible Graphene Electrodes for Prolonged Dynamic ECG Monitoring. *Sensors* **2016**, *16*, 1833, doi:10.3390/s16111833.
8. Xu, S.; Yang, D.; Zhang, F.; Liu, J.; Guo, A.; Hou, F. Fabrication of NiCo2O4 and Carbon Nanotube Nanocomposite Films as a High-Performance Flexible Electrode of Supercapacitors. *RSC Adv.* **2015**, *5*, 74032–74039, doi:10.1039/C5RA12855B.
9. Dou, B.; Li, J.; Jiang, B.; Yuan, R.; Xiang, Y. DNA-Templated In Situ Synthesis of Highly Dispersed AuNPs on Nitrogen-Doped Graphene for Real-Time Electrochemical Monitoring of Nitric Oxide Released from Live Cancer Cells. *Anal. Chem.* **2019**, *91*, 2273–2278, doi:10.1021/acs.analchem.8b04863.
10. Yang, X.-K.; Tang, Y.; Qiu, Q.-F.; Wu, W.-T.; Zhang, F.-L.; Liu, Y.-L.; Huang, W.-H. Aβ1–42 Oligomers Induced a Short-Term Increase of Glutamate Release Prior to Its Depletion As Measured by Amperometry on Single Varicosities. *Anal. Chem.* **2019**, *91*, 15123–15129, doi:10.1021/acs.analchem.9b03826.
11. Zhang, X.-W.; Qiu, Q.-F.; Jiang, H.; Zhang, F.-L.; Liu, Y.-L.; Amatore, C.; Huang, W.-H. Real-Time Intracellular Measurements of ROS and RNS in Living Cells with Single Core–Shell Nanowire Electrodes. *Angew. Chem. Int. Ed.* **2017**, *56*, 12997–13000, doi:10.1002/anie.201707187.
12. Huang, X.; Liu, Y.; Chen, K.; Shin, W.-J.; Lu, C.-J.; Kong, G.-W.; Patnaik, D.; Lee, S.-H.; Cortes, J.F.; Rogers, J.A. Stretchable, Wireless Sensors and Functional Substrates for Epidermal Characterization of Sweat. *Small* **2014**, *10*, 3083–3090, doi:10.1002/smll.201400483.
13. Kim, C.-L.; Jung, C.-W.; Oh, Y.-J.; Kim, D.-E. A Highly Flexible Transparent Conductive Electrode Based on Nanomaterials. *NPG Asia Mater.* **2017**, *9*, e438–e438, doi:10.1038/am.2017.177.
14. Kim, D.-H.; Lu, N.; Ma, R.; Kim, Y.-S.; Kim, R.-H.; Wang, S.; Wu, J.; Won, S.M.; Tao, H.; Islam, A.; et al. Epidermal Electronics. *Science* **2011**, *333*, 838–843, doi:10.1126/science.1206157.
15. Lien, D.-H.; Kao, Z.-K.; Huang, T.-H.; Liao, Y.-C.; Lee, S.-C.; He, J.-H. All-Printed Paper Memory. *ACS Nano* **2014**, *8*, 7613–7619, doi:10.1021/nn501231z.
16. Park, J.; Hwang, J.C.; Kim, G.G.; Park, J.-U. Flexible Electronics Based on One-Dimensional and Two-Dimensional Hybrid Nanomaterials. *InfoMat* **2020**, *2*, 33–56, doi:10.1002/inf2.12047.
17. Pavel, I.-A.; Lakard, S.; Lakard, B. Flexible Sensors Based on Conductive Polymers. *Chemosensors* **2022**, *10*, 97, doi:10.3390/chemosensors10030097.
18. Wang, B.-Y.; Yoo, T.-H.; Lim, J.W.; Sang, B.-I.; Lim, D.-S.; Choi, W.K.; Hwang, D.K.; Oh, Y.-J. Enhanced Light Scattering and Trapping Effect of Ag Nanowire Mesh Electrode for High Efficient Flexible Organic Solar Cell. *Small* **2015**, *11*, 1905–1911, doi:10.1002/smll.201402161.
19. Xue, T.; Sheng, Y.; Xu, J.; Li, Y.; Lu, X.; Zhu, Y.; Duan, X.; Wen, Y. In-Situ Reduction of Ag+ on Black Phosphorene and Its NH2-MWCNT Nanohybrid with High Stability and Dispersibility as Nanozyme Sensor for Three ATP Metabolites. *Biosens. Bioelectron.* **2019**, *145*, 111716, doi:10.1016/j.bios.2019.111716.

20. Zhu, X.; Lin, L.; Wu, R.; Zhu, Y.; Sheng, Y.; Nie, P.; Liu, P.; Xu, L.; Wen, Y. Portable Wireless Intelligent Sensing of Ultra-Trace Phytoregulator α-Naphthalene Acetic Acid Using Self-Assembled Phosphorene/Ti3C2-MXene Nanohybrid with High Ambient Stability on Laser Induced Porous Graphene as Nanozyme Flexible Electrode. *Biosens. Bioelectron.* **2021**, *179*, 113062, doi:10.1016/j.bios.2021.113062.
21. Lee, C.-S.; Ju, Y.; Kim, J.; Kim, T.H. Electrochemical Functionalization of Single-Walled Carbon Nanotubes with Amine-Terminated Dendrimers Encapsulating Pt Nanoparticles: Toward Facile Field-Effect Transistor-Based Sensing Platforms. *Sens. Actuators B Chem.* **2018**, *275*, 367–372, doi:10.1016/j.snb.2018.08.030.
22. Oh, J.-W.; Heo, J.; Kim, T.H. An Electrochemically Modulated Single-Walled Carbon Nanotube Network for the Development of a Transparent Flexible Sensor for Dopamine. *Sens. Actuators B Chem.* **2018**, *267*, 438–447, doi:10.1016/j.snb.2018.04.048.
23. Galadari, S.; Rahman, A.; Pallichankandy, S.; Thayyullathil, F. Reactive Oxygen Species and Cancer Paradox: To Promote or to Suppress? *Free Radic. Biol. Med.* **2017**, *104*, 144–164, doi:10.1016/j.freeradbiomed.2017.01.004.
24. Schumacker, P.T. Reactive Oxygen Species in Cancer: A Dance with the Devil. *Cancer Cell* **2015**, *27*, 156–157, doi:10.1016/j.ccell.2015.01.007.
25. Brewer, A.C.; Mustafi, S.B.; Murray, T.V.A.; Rajasekaran, N.S.; Benjamin, I.J. Reductive Stress Linked to Small HSPs, G6PD, and Nrf2 Pathways in Heart Disease. *Antioxid. Redox Signal.* **2013**, *18*, 1114–1127, doi:10.1089/ars.2012.4914.
26. Galaris, D.; Skiada, V.; Barbouti, A. Redox Signaling and Cancer: The Role of "Labile" Iron. *Cancer Lett.* **2008**, *266*, 21–29, doi:10.1016/j.canlet.2008.02.038.
27. Li, Z.; Xin, Y.; Wu, W.; Fu, B.; Zhang, Z. Topotactic Conversion of Copper(I) Phosphide Nanowires for Sensitive Electrochemical Detection of H2O2 Release from Living Cells. *Anal. Chem.* **2016**, *88*, 7724–7729, doi:10.1021/acs.analchem.6b01637.
28. Lin, M.T.; Beal, M.F. Mitochondrial Dysfunction and Oxidative Stress in Neurodegenerative Diseases. *Nature* **2006**, *443*, 787–795, doi:10.1038/nature05292.
29. Pramanik, D.; Dey, S.G. Active Site Environment of Heme-Bound Amyloid β Peptide Associated with Alzheimer's Disease. *J. Am. Chem. Soc.* **2011**, *133*, 81–87, doi:10.1021/ja1084578.
30. Genç, F.; Milcheva, N.P.; Hristov, D.G.; Gavazov, K.B. A Simple Cloud Point Extraction-Spectrophotometric Method for Total Vanadium Determination Using 4-(2-Thiazolylazo)Resorcinol and H2O2. *Chem. Pap.* **2020**, *74*, 1891–1901, doi:10.1007/s11696-019-01038-8.
31. Gupta, V.; Mahbub, P.; Nesterenko, P.N.; Paull, B. A New 3D Printed Radial Flow-Cell for Chemiluminescence Detection: Application in Ion Chromatographic Determination of Hydrogen Peroxide in Urine and Coffee Extracts. *Anal. Chim. Acta* **2018**, *1005*, 81–92, doi:10.1016/j.aca.2017.12.039.
32. Jia, Y.; Sun, S.; Cui, X.; Wang, X.; Yang, L. Enzyme-like Catalysis of Polyoxometalates for Chemiluminescence: Application in Ultrasensitive Detection of H2O2 and Blood Glucose. *Talanta* **2019**, *205*, 120139, doi:10.1016/j.talanta.2019.120139.
33. Liu, J.-W.; Luo, Y.; Wang, Y.-M.; Duan, L.-Y.; Jiang, J.-H.; Yu, R.-Q. Graphitic Carbon Nitride Nanosheets-Based Ratiometric Fluorescent Probe for Highly Sensitive Detection of H2O2 and Glucose. *ACS Appl. Mater. Interfaces* **2016**, *8*, 33439–33445, doi:10.1021/acsami.6b11207.
34. Ma, Y.; Cen, Y.; Sohail, M.; Xu, G.; Wei, F.; Shi, M.; Xu, X.; Song, Y.; Ma, Y.; Hu, Q. A Ratiometric Fluorescence Universal Platform Based on N, Cu Codoped Carbon Dots to Detect Metabolites Participating in H2O2-Generation Reactions. *ACS Appl. Mater. Interfaces* **2017**, *9*, 33011–33019, doi:10.1021/acsami.7b10548.
35. Shen, R.; Liu, P.; Zhang, Y.; Yu, Z.; Chen, X.; Zhou, L.; Nie, B.; Żaczek, A.; Chen, J.; Liu, J. Sensitive Detection of Single-Cell Secreted H2O2 by Integrating a Microfluidic Droplet Sensor and Au Nanoclusters. *Anal. Chem.* **2018**, *90*, 4478–4484, doi:10.1021/acs.analchem.7b04798.
36. Balasubramanian, P.; Annalakshmi, M.; Chen, S.-M.; Sathesh, T.; Peng, T.-K.; Balamurugan, T.S.T. Facile Solvothermal Preparation of Mn2CuO4 Microspheres: Excellent Electrocatalyst for Real-Time Detection of H2O2 Released from Live Cells. *ACS Appl. Mater. Interfaces* **2018**, *10*, 43543–43551, doi:10.1021/acsami.8b18510.
37. Jin, G.H.; Ko, E.; Kim, M.K.; Tran, V.-K.; Son, S.E.; Geng, Y.; Hur, W.; Seong, G.H. Graphene Oxide-Gold Nanozyme for Highly Sensitive Electrochemical Detection of Hydrogen Peroxide. *Sens. Actuators B Chem.* **2018**, *274*, 201–209, doi:10.1016/j.snb.2018.07.160.
38. Li, X.; Liu, Y.; Zhu, A.; Luo, Y.; Deng, Z.; Tian, Y. Real-Time Electrochemical Monitoring of Cellular H2O2 Integrated with In Situ Selective Cultivation of Living Cells Based on Dual Functional Protein Microarrays at Au−TiO2 Surfaces. *Anal. Chem.* **2010**, *82*, 6512–6518, doi:10.1021/ac100807c.
39. Li, Y.; Huan, K.; Deng, D.; Tang, L.; Wang, J.; Luo, L. Facile Synthesis of ZnMn2O4@rGO Microspheres for Ultrasensitive Electrochemical Detection of Hydrogen Peroxide from Human Breast Cancer Cells. *ACS Appl. Mater. Interfaces* **2020**, *12*, 3430–3437, doi:10.1021/acsami.9b19126.

40. Sun, Y.; Luo, M.; Meng, X.; Xiang, J.; Wang, L.; Ren, Q.; Guo, S. Graphene/Intermetallic PtPb Nanoplates Composites for Boosting Electrochemical Detection of H2O2 Released from Cells. *Anal. Chem.* **2017**, *89*, 3761–3767, doi:10.1021/acs.analchem.7b00248.
41. Wang, T.; Zhu, H.; Zhuo, J.; Zhu, Z.; Papakonstantinou, P.; Lubarsky, G.; Lin, J.; Li, M. Biosensor Based on Ultrasmall MoS2 Nanoparticles for Electrochemical Detection of H2O2 Released by Cells at the Nanomolar Level. *Anal. Chem.* **2013**, *85*, 10289–10295, doi:10.1021/ac402114c.
42. Yu, Y.; Pan, M.; Peng, J.; Hu, D.; Hao, Y.; Qian, Z. A Review on Recent Advances in Hydrogen Peroxide Electrochemical Sensors for Applications in Cell Detection. *Chin. Chem. Lett.* **2022**, *33*, 4133–4145, doi:10.1016/j.cclet.2022.02.045.
43. Zhang, T.; Gu, Y.; Li, C.; Yan, X.; Lu, N.; Liu, H.; Zhang, Z.; Zhang, H. Fabrication of Novel Electrochemical Biosensor Based on Graphene Nanohybrid to Detect H2O2 Released from Living Cells with Ultrahigh Performance. *ACS Appl. Mater. Interfaces* **2017**, *9*, 37991–37999, doi:10.1021/acsami.7b14029.
44. Zhang, Y.; Bai, X.; Wang, X.; Shiu, K.-K.; Zhu, Y.; Jiang, H. Highly Sensitive Graphene–Pt Nanocomposites Amperometric Biosensor and Its Application in Living Cell H2O2 Detection. *Anal. Chem.* **2014**, *86*, 9459–9465, doi:10.1021/ac5009699.
45. Choe, Y.; Yu, J.-Y.; Son, Y.-O.; Park, S.-M.; Kim, J.-G.; Shi, X.; Lee, J.-C. Continuously Generated H2O2 Stimulates the Proliferation and Osteoblastic Differentiation of Human Periodontal Ligament Fibroblasts. *J. Cell. Biochem.* **2012**, *113*, 1426–1436, doi:10.1002/jcb.24017.
46. Hsieh, H.-J.; Liu, C.-A.; Huang, B.; Tseng, A.H.; Wang, D.L. Shear-Induced Endothelial Mechanotransduction: The Interplay between Reactive Oxygen Species (ROS) and Nitric Oxide (NO) and the Pathophysiological Implications. *J. Biomed. Sci.* **2014**, *21*, 3, doi:10.1186/1423-0127-21-3.
47. Waters, C.M. Reactive Oxygen Species in Mechanotransduction. *Am. J. Physiol.-Lung Cell. Mol. Physiol.* **2004**, *287*, L484–L485, doi:10.1152/ajplung.00161.2004.
48. Ahammad, A.J.S.; Lee, J.-J.; Rahman, M.A. Electrochemical Sensors Based on Carbon Nanotubes. *Sensors* **2009**, *9*, 2289–2319, doi:10.3390/s90402289.
49. Zhang, W.; Zhu, S.; Luque, R.; Han, S.; Hu, L.; Xu, G. Recent Development of Carbon Electrode Materials and Their Bioanalytical and Environmental Applications. *Chem. Soc. Rev.* **2016**, *45*, 715–752, doi:10.1039/C5CS00297D.
50. Abera, B.D.; Falco, A.; Ibba, P.; Cantarella, G.; Petti, L.; Lugli, P. Development of Flexible Dispense-Printed Electrochemical Immunosensor for Aflatoxin M1 Detection in Milk. *Sensors* **2019**, *19*, 3912, doi:10.3390/s19183912.
51. Zhou, Y.; Azumi, R. Carbon Nanotube Based Transparent Conductive Films: Progress, Challenges, and Perspectives. *Sci. Technol. Adv. Mater.* **2016**, *17*, 493–516, doi:10.1080/14686996.2016.1214526.
52. Agrisuelas, J.; González-Sánchez, M.-I.; Valero, E. Hydrogen Peroxide Sensor Based on in Situ Grown Pt Nanoparticles from Waste Screen-Printed Electrodes. *Sens. Actuators B Chem.* **2017**, *249*, 499–505, doi:10.1016/j.snb.2017.04.136.
53. Chen, X.; Wu, G.; Cai, Z.; Oyama, M.; Chen, X. Advances in Enzyme-Free Electrochemical Sensors for Hydrogen Peroxide, Glucose, and Uric Acid. *Microchim. Acta* **2014**, *181*, 689–705, doi:10.1007/s00604-013-1098-0.
54. Jiménez-Pérez, R.; González-Rodríguez, J.; González-Sánchez, M.-I.; Gómez-Monedero, B.; Valero, E. Highly Sensitive H2O2 Sensor Based on Poly(Azure A)-Platinum Nanoparticles Deposited on Activated Screen Printed Carbon Electrodes. *Sens. Actuators B Chem.* **2019**, *298*, 126878, doi:10.1016/j.snb.2019.126878.
55. Rahman, M.M.; Jeon, I.C. Studies of Electrochemical Behavior of SWNT-Film Electrodes. *J. Braz. Chem. Soc.* **2007**, *18*, 1150–1157, doi:10.1590/S0103-50532007000600008.
56. Heinemann, A.; Koenen, S.; Schwabe, K.; Rehbock, C.; Barcikowski, S. How Electrophoretic Deposition with Ligand-Free Platinum Nanoparticles Affects Contact Angle. *Key Eng. Mater.* **2015**, *654*, 218–223, doi:10.4028/www.scientific.net/KEM.654.218.
57. Goran, J.M.; Phan, E.N.H.; Favela, C.A.; Stevenson, K.J. H2O2 Detection at Carbon Nanotubes and Nitrogen-Doped Carbon Nanotubes: Oxidation, Reduction, or Disproportionation? *Anal. Chem.* **2015**, *87*, 5989–5996, doi:10.1021/acs.analchem.5b00059.
58. Sitta, E.; Gómez-Marín, A.M.; Aldaz, A.; Feliu, J.M. Electrocatalysis of H2O2 Reduction/Oxidation at Model Platinum Surfaces. *Electrochem. Commun.* **2013**, *33*, 39–42, doi:10.1016/j.elecom.2013.04.014.

59. Gao, W.; Liu, Y.; Zhang, H.; Wang, Z. Electrochemiluminescence Biosensor for Nucleolin Imaging in a Single Tumor Cell Combined with Synergetic Therapy of Tumor. *ACS Sens.* **2020**, *5*, 1216–1222, doi:10.1021/acssensors.0c00292.
60. Zhang, H.; Gao, W.; Liu, Y.; Sun, Y.; Jiang, Y.; Zhang, S. Electrochemiluminescence-Microscopy for MicroRNA Imaging in Single Cancer Cell Combined with Chemotherapy-Photothermal Therapy. *Anal. Chem.* **2019**, *91*, 12581–12586, doi:10.1021/acs.analchem.9b03694.